J Physiol 591.11 (2013) pp 2795–2812

The Journal of Physiology

Role of microprojections in myoendothelial feedback – a theoretical study

Sridevi Nagaraja[1], Adam Kapela[1], Cam H. Tran[2], Donald G. Welsh[2] and Nikolaos M. Tsoukias[1]

[1] *Department of Biomedical Engineering, Florida International University, Miami, FL, USA*
[2] *Hotchkiss Brain and Libin Cardiovascular Research Institute and Department of Physiology & Pharmacology, University of Calgary, Calgary, Alberta, Canada*

Key points

- Endothelial microprojections (MPs) are cellular extensions of endothelial cells (ECs) that may be involved in regulation of smooth muscle cell (SMC) constriction in blood vessels.
- We developed computational models to investigate the role of MPs in generating EC feedback during SMC stimulation. The models account for the geometry of MPs and heterogeneous distribution of membrane channels and receptors in an EC.
- Simulations show that SMC stimulation causes calcium release in and around EC MPs that activates hyperpolarizing currents in ECs and moderates SMC constriction.
- The results help us better understand the mechanisms that regulate blood flow and pressure.

Abstract We investigated the role of myoendothelial projections (MPs) in endothelial cell (EC) feedback response to smooth muscle cell (SMC) stimulation using mathematical modelling. A previously developed compartmental EC–SMC model is modified to include MPs as subcellular compartments in the EC. The model is further extended into a 2D continuum model using a finite element method (FEM) approach and electron microscopy images to account for MP geometry. The EC and SMC are coupled via non-selective myoendothelial gap junctions (MEGJs) which are located on MPs and allow exchange of Ca^{2+}, K^+, Na^+ and Cl^- ions and inositol 1,4,5-triphosphate (IP_3). Models take into consideration recent evidence for co-localization of intermediate-conductance calcium-activated potassium channels (IK_{Ca}) and IP_3 receptors (IP_3Rs) in the MPs. SMC stimulation causes an IP_3-mediated Ca^{2+} transient in the MPs with limited global spread in the bulk EC. A hyperpolarizing feedback generated by the localized IK_{Ca} channels is transmitted to the SMC via MEGJs. MEGJ resistance (R_{gj}) and the density of IK_{Ca} and IP_3R in the projection influence the extent of EC response to SMC stimulation. The predicted Ca^{2+} transients depend also on the volume and geometry of the MP. We conclude that in the myoendothelial feedback response to SMC stimulation, MPs are required to amplify the SMC initiated signal. Simulations suggest that the signal is mediated by IP_3 rather than Ca^{2+} diffusion and that a localized rather than a global EC Ca^{2+} mobilization is more likely following SMC stimulation.

(Received 5 December 2012; accepted after revision 23 March 2013; first published online 25 March 2013)
Corresponding author N. M. Tsoukias: Department of Biomedical Engineering, Florida International University, 10555 W. Flagler Street, EC 2674, Miami, FL 33174. USA. Email: tsoukias@fiu.edu

Abbreviations ACh, acetylcholine; CICR, calcium-induced calcium release; EC, endothelial cell; EDHF, endothelium-derived hyperpolarizing factor; EDRF, endothelium-derived relaxing factor; ER, endoplasmic reticulum; FEM, finite element method; IK_{Ca}, intermediate-conductance Ca^{2+}-activated K^+ channels; IP_3, inositol 1,4,5-triphosphate; IP_3R, IP_3 receptor; MEGJ, myoendothelial gap junctions; MP, myoendothelial projection; NA, noradrenaline; SMC, smooth muscle cell.

DOI: 10.1113/jphysiol.2012.248948

Introduction

Myoendothelial communication plays an important role in vascular tone regulation. Complex bidirectional pathways exist between the endothelial cell (EC) and smooth muscle cell (SMC) layers which regulate SMC constriction and vessel diameter. Agonist stimulation of SMCs may lead to a calcium (Ca^{2+}) response in ECs sufficient to initiate Ca^{2+}-dependent vasodilatory signals such as the endothelium-derived hyperpolarizing factor (EDHF). Such EC response can moderate SMC constriction and is referred to as myoendothelial feedback. The presence of endothelial feedback after SMC stimulation was first suggested by Dora *et al.* (1997) and remains a topic of active investigation (Dora *et al.* 2008; Ledoux *et al.* 2008*a*; Sandow *et al.* 2009*b*; Tran *et al.* 2012). Different aspects of this feedback response remain unresolved including the identity of the main mediator in SMC-to-EC communication (Ca^{2+} or inositol 1,4,5-triphosphate (IP_3)) and the characteristics of the EC response, as well as whether attenuation of this mechanism contributes to vessel pathology (Sandow *et al.* 2009*b*; Kerr *et al.* 2012).

Myoendothelial projections (MPs) are cellular extensions from ECs and/or SMC that extend over the internal elastic lamina and come in close contact with the other cell type (Heberlein *et al.* 2009; Sandow *et al.* 2009*b*). In spite of their early discovery in 1957 (Moore & Ruska, 1957), the functional importance of MPs has only recently begun to be appreciated (Kerr *et al.* 2012). Electron microscopy studies confirm the presence of MPs in many different vessels, including in rat mesenteric arteries (Ledoux *et al.* 2008*a*; Sandow *et al.* 2009*b*; Tran *et al.* 2012). MPs vary both in number and size among different vascular beds, age, species, sex and diseased states of animals (Sandow *et al.* 2009*a*). An increase in incidences of MPs with decrease in vessel diameter is often reported (Heberlein *et al.* 2009; Sandow *et al.* 2009*a*), which correlates with an increase in EDHF action (Garland *et al.* 1995; Shimokawa *et al.* 1996; Hill *et al.* 2000, 2002) but not with the activity of the endothelium-derived relaxing factor (EDRF) whose efficacy often diminishes with decrease in vessel size (Luksha *et al.* 2009).

Recent immunohistochemical labelling studies show evidence for localization of IP_3 receptors (IP_3Rs), intermediate conductance Ca^{2+}-activated potassium channels (IK_{Ca}) and connexins in MPs (Crane *et al.* 2003; Sandow *et al.* 2006; Dora *et al.* 2008; Isakson, 2008; Ledoux *et al.* 2008*a*; Sandow *et al.* 2009*b*). Myoendothelial gap junctions (MEGJs) are often located on top of these projections and are responsible for electrochemical communication between ECs and SMCs (Heberlein *et al.* 2009; Sandow *et al.* 2009*a*,*b*). It has been proposed that a small amount of IP_3 and/or Ca^{2+} entering from the stimulated SMC can accumulate in the restricted space of MPs and activate localized IP_3Rs, leading to rapid release of Ca^{2+} from the endoplasmic reticulum (ER) stores and amplification of Ca^{2+} response. In support of this theory, spontaneous and agonist initiated local Ca^{2+} events like 'pulsars' (Ledoux J, 2008*b*) and 'wavelets' (Tran *et al.* 2012) have been shown to occur in and around MP sites in ECs following both EC as well as SMC stimulation. The occurrence of these Ca^{2+} events in the vicinity of localized IK_{Ca} channels is consistent with a role for the EDHF in closing the myoendothelial feedback loop. Endothelial nitric oxide synthase (eNOS) may also colocalize at MPs, but evidence indicates a limited role for NO in the feedback response (Nausch *et al.* 2012).

Mathematical modelling can assist in further analysis of the experimental data, but few theoretical studies have investigated EC–SMC communication. In a recent study, Brasen *et al.* (2012) describe a 2D-axisymmetric model incorporating the anatomical structure of MPs to show the spatiotemporal modulation of Ca^{2+} and IP_3 in EC, SMC and MPs during EC and SMC stimulation. In this model, they highlight the competence of MPs in rectification of Ca^{2+} signals by the virtue of their structure and location. However, the role of the membrane potential (V_m), the effect of plasma membrane channels, the localization of channels and receptors, and the myoendothelial feedback in the heterocellular communication have yet to be modelled. In our previously developed EC–SMC model (Kapela *et al.* 2009), we integrated detailed single cell EC (Silva *et al.* 2007) and SMC (Kapela *et al.* 2008) models with electrical, chemical and NO coupling pathways. Agonist stimulation of ECs increased Ca^{2+} in ECs, activated EDHF and EDRF pathways, hyperpolarized SMC, and reduced SMC Ca^{2+}. Ca^{2+} fluxes from stimulated SMC or EC did not elevate global Ca^{2+} in the other cell. EC feedback response to SMC stimulation was observed only when we significantly increased gap junction permeability to IP_3 and EC IP_3R density relatively to previously suggested values.

In this study, we develop computational models to investigate the role of MPs in myoendothelial communication. We extend our previously developed EC–SMC model to incorporate a subcompartment within the EC that simulates the presence of MPs (Fig. 1*A*). We also present a continuum model capable of incorporating accurate MP geometry from electron microscopy images (Fig. 2*A*) and account for spatial localization of IK_{Ca} and IP_3Rs as suggested in experimental studies (Crane *et al.* 2003; Sandow *et al.* 2006; Isakson, 2008; Ledoux *et al.* 2008*a*). The current models provide theoretical insights into the role of MPs.

Methods

Compartmental model

The current model is based on our previously developed two-cell EC–SMC model (Kapela *et al.* 2009). The earlier models were optimized for a specific tissue (i.e. model descriptions and parameters were based on experimental data obtained primarily from rat mesenteric resistance arteries). We modified the EC by partitioning it into two compartments representing the bulk EC and the MP as shown in Fig. 1*A*. Parametric studies were performed to determine the influence of certain parameters on model responses.

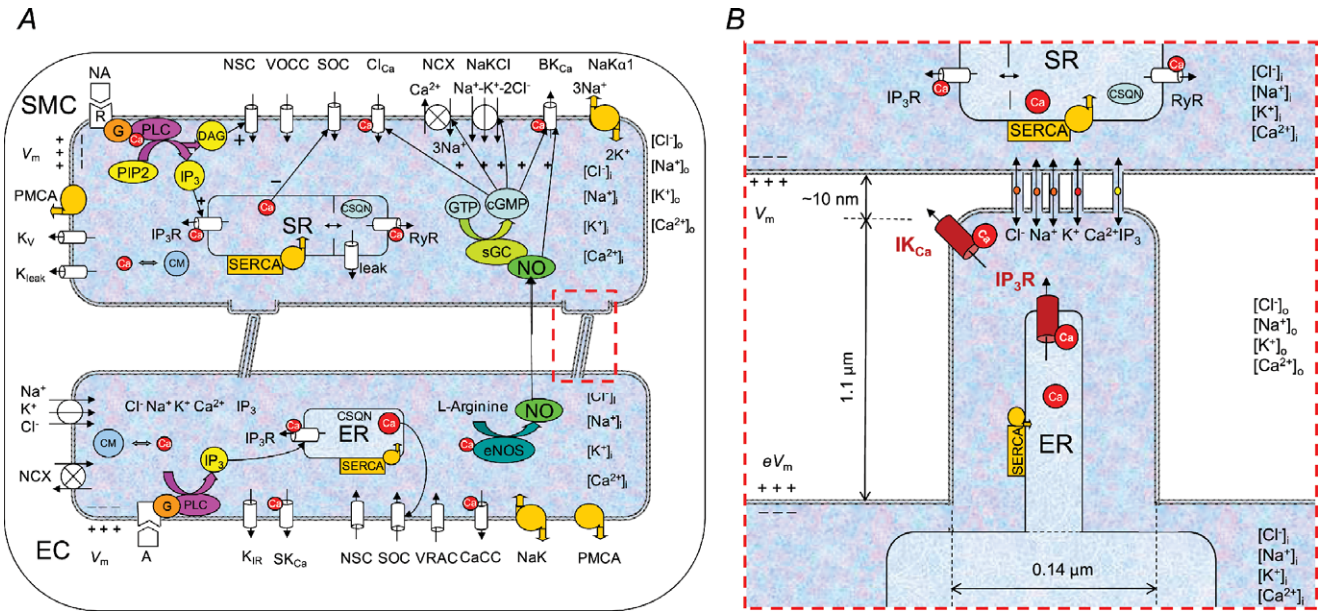

Figure 1.
A, schematic diagram showing all the channels and pumps incorporated in the EC–MP–SMC compartmental model. *B*, characteristics of the EC microprojections (MP). Localized (high density) IK_{Ca} channels and IP_3Rs are present in the MP. All other channels and pumps are distributed proportionally to the volumes of the EC bulk and MP (the other channels in MP are not shown for clarity).

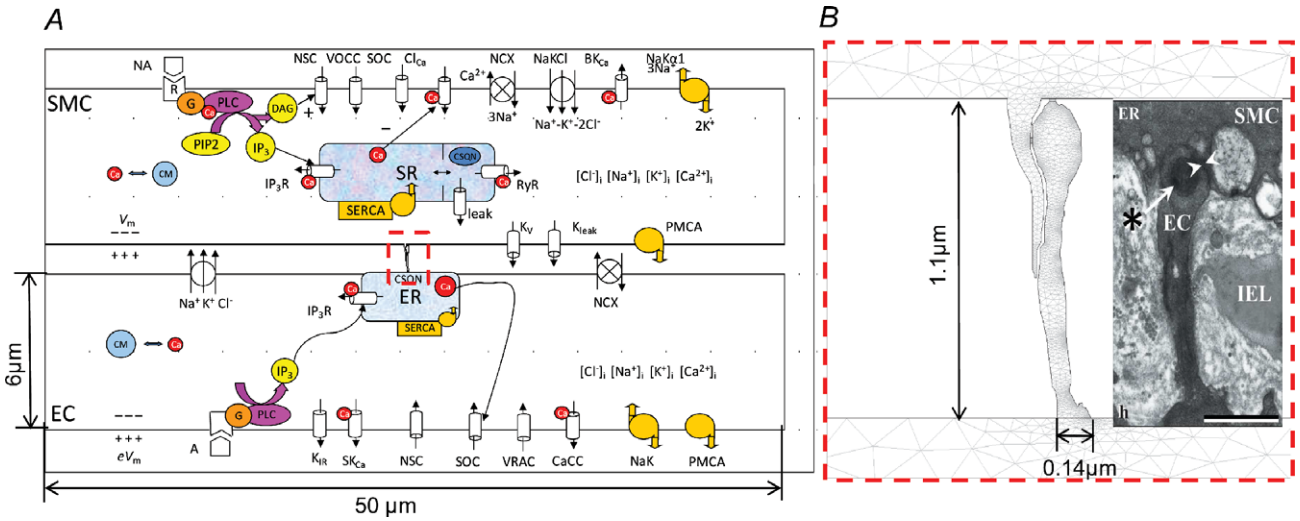

Figure 2.
A, 2D FEM model geometry with SMC and EC as rectangular segments and with a MP whose shape is imported from electron microscopy image by (Sandow *et al.* 2009*b*) (inset in *B*). Ion channel currents are uniformly distributed along the top and bottom boundaries of each cell. *B*, EC projection with mesh. IK_{Ca} channels and IP_3Rs are localized in the MP. All other channels and pumps are also present in MP membrane, but proportionally to MP volume. The ER is homogeneously spread across the entire EC including the MPs.

Table 1. List of parameters describing dimensions of MPs and microdomains along with values of diffusion constants of ions and IP_3 in the cytosol

Parameter	Value	Description
G_{IKCa}	Bulk EC: 0.0 nS MP: 1.72 nS (Kapela *et al.* 2009)	Maximum IK_{Ca} channel conductance
$I_{IP3R,max}$	Bulk EC: 1.053 $\times 10^3$ pA mM^{-1} MP: 0.117 $\times$ 10^3 pA mM^{-1}	Maximum current through IP_3R per concentration difference
K_{d_act}	Low: 130 nM (Jacobsen *et al.* 2007) High: 350 nM (assumed)	$[Ca^{2+}]$ for half-maximal activation of IP_3R
f	Control: 1.75 No MP : 10^{-3}	Diffusional restriction between MP and bulk EC
D_{Ca}	300 μm^2 s^{-1} (Allbritton *et al.* 1992)	Diffusivity of free calcium in cytosol
D_K	744 μm^2 s^{-1}	Diffusivity of potassium in cytosol
D_{Na}	505 μm^2 s^{-1}	Diffusivity of sodium in cytosol
D_{Cl}	900 μm^2 s^{-1}	Diffusivity of chloride in cytosol
D_{IP3}	283 μm^2 s^{-1} (Allbritton *et al.* 1992)	Diffusivity of IP_3 in cytosol
A_{mp}	0.0154 μm^2 (Sandow & Hill, 2000)	Area of a single MP
L_{mp}	3.5 μm (Sandow & Hill, 2000)	Diffusion length from MP to bulk EC
N_{mp}	2.7 (Dora *et al.* 2008)	Number of MEGJ/EC
F	96487.0 C mol^{-1}	Faraday's constant
R	8341 mJ (mol K)$^{-1}$	Universal gas constant
T	293 K	Temperature
z_K, z_{Na}, z_{Ca}, z_{Cl}	1, 1, 2, –1	Ion valency of K^+, Na^+, Ca^{2+}, Cl^-

Geometric parameters

Figure 1*B* shows the dimensions used to calculate effective volume, area and diffusion parameters for the EC MP compartment. The length and width of MPs are taken from electron microscopy images of rat mesenteric artery (Sandow *et al.* 2009*b*). 2.7 MEGJs per endothelial cell were assumed (Dora *et al.* 2008) and that every projection contains one gap junction. The total EC volume (1 pl; Schuster *et al.* 2003) is divided into bulk EC volume and a much smaller MP volume. MP volume is calculated by assuming the MP to be cylindrically shaped with dimensions as shown in Fig. 1*B*. Membrane area, whole cell capacitance and the ER/SR are divided between the two compartments proportionally to their volume ratios. This allows for appropriate division of intracellular fluxes between the two compartments.

Ionic channel distributions

The model schematic is shown in Fig. 1*A*. The whole cell conductances of the channels and pumps are maintained the same as in the previous EC and SMC models (Silva *et al.* 2007; Kapela *et al.* 2008). The following channels are assumed uniformly distributed across the membrane of EC and their maximum conductances are scaled by the bulk and MP volumes: Inwardly rectifying potassium channel (K_{ir}), non-selective cation channel (NSC), small conductance calcium activated potassium channel (SK_{Ca}), store-operated channel (SOC), calcium activated chloride channel (CaCl), sodium-potassium pump ($NaK_{\alpha 1}$), Na^+–Ca^{2+}exchanger (NCX), plasma membrane Ca^{2+}-ATPase (PMCA), sarco(endo)plasmic reticulum Ca^{2+}-ATPase (SERCA). IK_{Ca} (Crane *et al.* 2003; Sandow *et al.* 2006, 2009*b*; Dora *et al.* 2008; Ledoux *et al.* 2008*a*) and IP_3R (Isakson, 2008; Ledoux *et al.* 2008*a*; Sandow *et al.* 2009*b*) are localized to MPs as shown in Fig. 1*B*. The maximum conductance of IK_{Ca} channel (G_{IKCa}) has been measured in porcine arteries (Bychkov *et al.* 2002), and was rescaled in our lumped EC model (Silva *et al.* 2007). Immunohistochemistry data suggest a high presence of IK_{Ca} channels and IP_3Rs in the vicinity of MPs (Sandow *et al.* 2006; Dora *et al.* 2008; Isakson, 2008; Ledoux *et al.* 2008*a*; Sandow *et al.* 2009*b*). IK_{Ca} labelling is very punctuated and colocalized with MPs in some vascular beds, e.g. rat mesenteric arteries (Dora *et al.* 2008; Ledoux *et al.* 2008*a*; Sandow *et al.* 2009*b*), but more dispersed in others (McNeish *et al.* 2006; Tran *et al.* 2012) and therefore their distribution between MPs and the rest of the cell is likely to vary. Thus, under control conditions we assume that the majority of IK_{Ca} channels are concentrated in MPs (Table 1) and we also performed simulations for different levels of IK_{Ca} localization. Similarly, a significant percentage (i.e. 10% under control conditions) of the total IP_3Rs is assumed to be localized inside the MPs and the remaining distributed in the bulk of EC. This corresponds to a much higher IP_3R density in MP than in the bulk of EC. (The distribution of IP_3Rs is controlled by the maximum current parameter ($I_{IP3R,max}$, Table 1).) The degree of localization (10%) was assumed based on the fact that

IP_3Rs are not as highly colocalized with MPs as IK_{Ca} (Ledoux *et al.* 2008*a*; Sandow *et al.* 2009*b*). In the SMC model, single cytosolic compartment integrates currents through the following channels: voltage-dependent L-type calcium channel (VOCC), delayed rectifier potassium channel (K_v), NSC, ATP activated potassium channel (K_{ATP}), large conductance calcium activated potassium channel (BK_{Ca}), SOC, CaCl, NCX, and PMCA and $NaK_{\alpha 1}$ pumps. Norepinephrine (NA) stimulation generates IP_3 through Ca^{2+}-dependent phospholipase-C (PLC). MEGJs connect the MP compartment to the SMC (Sandow & Hill, 2000; Dora *et al.* 2003). Permeability of gap junctions is calculated based on experimental data for the total MEGJ resistance (R_{gj}; Yamamoto *et al.* 2001). MEGJs are assumed to be non-selective and permeable to Na^+, K^+, Ca^{2+}, Cl^- ions and IP_3. The EDRF–NO pathway is blocked for all simulations.

Coupling between MPs and bulk EC: diffusion currents

We used (electro) diffusion equations to describe fluxes of the four ions and IP_3. The equations account for fluxes between two compartments and their dependence on V_m as well as concentration difference:

$$I_S = z_S \times F \times P_S^{b-mp} \times N_{mp} \times \left(([S]_{bulk} - [S]_{mp}) + \frac{z_S \times F \times ([S]_{bulk} + [S]_{mp})}{2 \times R \times T} \times (V_{m,bulk} - V_{m,mp}) \right), \quad (1)$$

$$J_{IP3} = P_{IP3}^{b-mp} \times N_{mp} \times \left([IP_3]_{bulk} - [IP_3]_{mp} \right), \quad (2)$$

where S represents Na^+, K^+, Ca^{2+} and Cl^-. Suffixes 'mp' and 'bulk' represent the MP and bulk compartments in EC. P_S^{b-MP} is the permeability of species S between the MP and the bulk of the cell. A first approximation for its value can be acquired from the species diffusivity (D_s), MP cross-sectional area (A_{mp}) and the MP length (L_{mp}), i.e.

$$P_S^{b-MP} = \frac{D_s \times A_{mp}}{f \times L_{mp}}.$$

A correction factor (f) was also utilized to account for the effects of buffering/degradation/extrusion and/or the presence of subcellular organelles that can further limit the exchange of species between the two compartments.

The ER in MP is coupled with the bulk ER using diffusion equation for Ca^{2+} transport:

$$I_{diff} = z_{Ca} \times F \times D_{Ca} \times A_{mp} \times N_{mp} \times \frac{([Ca]_{s,bulk} - [Ca]_{s,mp})}{L_{mp}}, \quad (3)$$

where $[Ca]_s$ is the concentration of Ca^{2+} in the ER stores. All parameter values and their description are listed in Table 1.

Calcium-induced calcium release (CICR)

The default IP_3R kinetics in the EC bulk and MP is the same as in the previous EC-SMC model (Silva *et al.* 2007; Kapela *et al.* 2009), comprising of IP_3-dependent activation and Ca^{2+}-dependent inactivation terms:

$$I_{IP3R} = I_{IP3R,max} \times \frac{[IP_3]^{3.8}}{[IP_3]^{3.8} + [K_{m,IP3}]^{3.8}} \times \frac{K_{i,Cai}^{3.8}}{[Ca]_i^{3.8} + K_{i,Cai}^{3.8}} \times ([Ca]_S - [Ca]_i), \quad (4)$$

where $[Ca]_S$ and $[Ca]_i$ represent the ER and cytosolic calcium concentrations respectively and $[IP_3]$ represents intracellular IP_3 concentration. $K_{m,IP3}$ and $K_{i,Cai}$ are the half-activation and -inhibition constants for IP_3 activation and Ca^{2+}-dependent inhibition of the IP_3R current.

To test the potential of intercellular Ca^{2+} flux to induce CICR through IP_3Rs, the IP_3R current in the EC was modified to include a calcium-dependent activation component (P_{Ca}) as shown in eqns (5) and (6).

$$I_{IP3R} = I_{IP3R,max} \times \frac{[IP_3]^{3.8}}{[IP_3]^{3.8} + [K_{m,IP3}]^{3.8}} \times P_{Ca\_act} \times P_{Ca\_inact} \times ([Ca]_S - [Ca]_i), \quad (5)$$

$$P_{Ca\_act} = \frac{[Ca]_i^4}{K_{d\_act}^4 + [Ca]_i^4}, \quad P_{Ca\_inact} = \frac{K_{i,Cai}^{3.8}}{[Ca]_i^{3.8} + K_{i,Cai}^{3.8}}. \quad (6)$$

Two values of K_{d_act} were examined as listed in Table 1. The lower value of K_{d_act} was taken from a model of SMCs (Jacobsen *et al.* 2007), and the second value is an average from various cell types (Finch *et al.* 1991; Atri *et al.* 1993).

Numerical methods

All other model equations are described in detail in previous studies (Silva *et al.* 2007; Kapela *et al.* 2008, 2009). The compartmental EC and SMC models are implemented using 20 and 26 ordinary differential equations, respectively. Table 1 lists any changed or newly introduced parameter values. The rest of the parameter values remain unchanged from the previous EC–SMC model. The equations are coded in Fortran 90 and solved numerically using Gear's backward differentiation formula method for stiff systems (IMSL Numerical Library routine). The maximum time step was 1 ms and the tolerance for convergence was 0.0005.

Finite element method (FEM) model

The compartmental EC–MP model described above does not allow us to predict intracellular concentration

gradients, the spatiotemporal nature of Ca^{2+} mobilization and the localization of the Ca^{2+} signal. Furthermore, preliminary simulations revealed that the feedback response depends significantly on the permeability between the MP and the bulk EC cytosol (adjusted through the factor 'f''). Calculation of fluxes between two unequal compartments (MP and bulk EC) needs to take into account a variable diffusion area, boundary fluxes, buffering of Ca^{2+} and degradation of IP_3 which are difficult to accurately capture through lumped diffusion parameters used in the compartmental model. Thus, we developed a FEM model to account for the spatial gradients of Ca^{2+} inside the EC MP and for the diffusion of species from the MP to the bulk EC with higher accuracy. A 2D model also allows us to incorporate accurate MP geometry by importing MP images from experimental studies and to account for spatial localizations of IK_{Ca} and IP_3Rs within the MPs.

The model is developed using the Chemical Engineering module of COMSOL, similarly to (Kapela & Tsoukias, 2011). While a 3D cylindrical axisymmetric model of EC and SMC was implemented in (Kapela & Tsoukias, 2011), here we assumed a simplified geometry and EC and SMC are represented as rectangular structures with dimensions as shown in Fig. 2*A*. The model implements only half of the EC and SMC. The results in the remaining half are assumed to be symmetrical. The shapes of the projections are imported from experimental electron microscopy images (Heberlein *et al.* 2009; Sandow *et al.* 2009*b*; Tran *et al.* 2012; Fig. 5). Volume of MP is calculated assuming the MP to be cylindrical with diameter and length as shown in Fig. 2*B*. Two rectangular domains connect the SMC and EC MPs to represent MEGJs. Differences in height (depth) of the cell's bulk, MPs, and MEGJs have been accounted for by appropriate scaling of fluxes at the boundaries between MEGJ and MP and at boundary between MP and bulk cytosol.

Nernst-Planck equations describe the electrodiffusion of the ions in the EC, MP, SMC and MEGJs:

$$\delta_{ts}\frac{\partial[S]}{\partial t} + \nabla(-D_S \times \nabla[S] - z_S \times u_{mS} \times F \times [S] \times \nabla V) = R_s, \quad (7)$$

where $[S]$ is the intracellular concentration of the four ionic species (Ca^{2+}, Na^+, K^+, Cl^-), D_s is the diffusivity of the respective ions, ∇V is the electrical gradient, z_S is the charge, F is the Faraday constant, and u_{mS} is the mobility of the respective ion. R_s is the source/sink term which includes expressions for Ca^{2+} release/uptake from the ER/SR, and Ca^{2+} buffering in EC bulk and MP. In SMC, fast Ca^{2+} buffering is represented by the Ca^{2+}-dependent function δ_{ts}. Diffusion of IP_3 and buffered Ca^{2+} in the cytosol, and Ca^{2+} in ER/SR is implemented using diffusion equations inside the SMC, EC, MP and MEGJs domains:

$$\delta_{ts}\frac{\partial[S]}{\partial t} + \nabla(-D_S \times \nabla[S]) = R_s, \quad (8)$$

where $[S]$ is the concentration of either species (IP_3, Ca^{2+}_S, $Ca^{2+}{}_{buffered}$). In EC, IP_3 production is introduced by the R_s term, while in SMC agonist receptors and IP_3 formation are described by an embedded weak boundary equation.

All model equations describing the membrane and store channels are the same as in the compartmental model. The membrane currents are defined as boundary fluxes across the top and bottom boundaries of EC, SMC and all boundaries of the MP. The left and right boundaries of the cell are assumed insulated. To distribute the channels uniformly, the currents are divided between the MP and bulk cytosol according to the volumes of MP and bulk cytosol. Similarly to the compartmental model, the whole maximum conductance of IK_{Ca} channels (G_{IKCa}) and 10% of IP_3R_{max} current were placed in EC MPs. 900 MΩ is used as control R_{gj} unless stated otherwise.

The equations are solved using the SPOOLES direct solver with absolute and relative tolerances of 10^{-3} and 10^{-2} respectively. The solution time was 30 s with a time stepping of 0.1 s. The different geometries were divided into ∼1000 elements. Unless stated otherwise, the NO pathway is blocked for all simulations.

Results

Global *vs.* local Ca^{2+} and IP_3 changes

Figure 3 shows Ca^{2+} and IP_3 changes in bulk EC and MP compartments during SMC (Fig. 3*A*) and EC (Fig. 3*B*) agonist stimulations. Following SMC stimulation with NA (Fig. 3*A*), the IP_3 diffusing from SMC into the EC MP causes a high IP_3 transient in the MP, which does not spread into the bulk of EC. A large Ca^{2+} transient is generated in the MP by activation of IP_3Rs localized in the MP. Like IP_3, Ca^{2+} in the MP does not spread much into the bulk EC compartment. IK_{Ca} channels localized in the MPs are activated by the Ca^{2+} transients and generate hyperpolarizing current that spreads through gap junctions to moderate SMC depolarization (Fig. 3*C*). The high Ca^{2+} and IP_3 transients in the MP after NA stimulation of SMC are attributed to the small volume of the MP, the localization of IP_3Rs and the restricted diffusion between the MP and bulk EC. Thus, the magnitude of the Ca^{2+} and IP_3 transients depend on the assumed value of effective permeability P_S^{b-mp}. Simulations with a wide range of permeability values were performed by varying parameter f (data not shown). Correction factor $f < 0.1$ makes the bulk and MP well mixed and effectively lacking a functional MP compartment, while $f \gg 1.75$

(control) creates excessive electrical resistance and the two compartments are no longer near isopotential.

Acetylcholine (ACh) stimulation of bulk EC compartment increases the global Ca^{2+} concentration through the production of IP_3 (Fig. 3*B*) and opening of IP_3Rs in ER. Diffusion of IP_3 from the bulk to MP generates a Ca^{2+} increase ~7 times higher than in bulk EC because of the localization of IP_3Rs in the small volume of MPs and restricted diffusion between the two compartments. The Ca^{2+} increase in the bulk and MP compartments opens SK_{Ca} and IK_{Ca} channels and hyperpolarizes the EC. This change in EC V_m is transmitted through MEGJs as EDHF and hyperpolarizes SMC (Fig. 3*D*).

In agreement with the compartmental model, the 2D FEM model predicts that NA stimulation of SMC generates high IP_3 (Fig. 4*C*) and Ca^{2+} (Fig. 4*A*) transients inside the EC MP with minimal spread into the bulk EC. Simulations with ACh stimulation (Fig. 4*B* and *D*) are also consistent with the compartmental model (Fig. 3*B*). In Fig. 5, we examined the effect of MP geometry on the spread of Ca^{2+} from the MP into the bulk EC. The three MP geometries examined are from the electron microscopy studies of rat mesenteric arteries (Sandow *et al.* 2009*b*), mouse cremaster arterioles (Heberlein *et al.* 2009), and hamster vessels (Tran *et al.* 2012). Under control MP volume, the long MP with comparatively small diffusion area yielded a large Ca^{2+} transient which did not spread much into the bulk of EC (Fig. 5*A*). The transients decreased with smaller heights and larger surface areas of the MPs (Fig. 5*B* and *C*). The short MP with large surface area did not have a significant Ca^{2+} transient in the MP (Fig. 5*B*). If the volume of each MP was reduced 5 times, effectively making it flatter, the predicted Ca^{2+} transients in the MPs increased significantly in all three cases (Fig. 5*D*–*F*), but the MP with higher surface area (Fig. 5*E*) allowed for a comparatively bigger spread of Ca^{2+} into the bulk of EC.

Effect of MPs

Figure 6 shows the effect of EC MPs on feedback in SMC V_m. In the presence of MPs, an approximately 2–3 mV feedback can be achieved, compared to the model with a single well-mixed EC compartment (Fig. 6*A*, continuous *vs.* dashed lines). The feedback is lost in the model without MPs because NA cannot generate a Ca^{2+} transient in the single compartment model (Fig. 6*B*, dashed *vs.* continuous lines). In fact, the global EC Ca^{2+} decreases in the model without MPs (Fig. 6*B*, dashed line) because of SMC

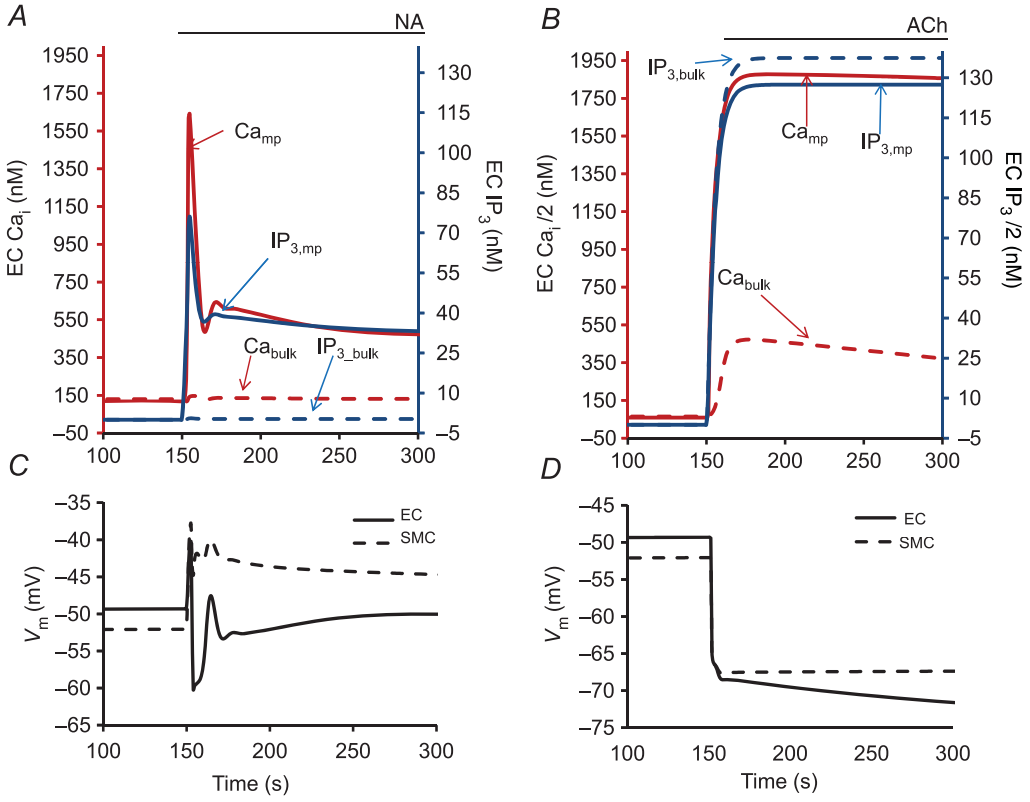

Figure 3.
Compartmental model results showing Ca^{2+} and IP_3 concentrations in the EC MP (continuous lines) and EC bulk (dashed lines) during 1 μM NA stimulation of SMC (*A*) and ACh stimulation of EC (*B*). Corresponding V_m in EC (continuous lines) and SMC (dashed lines) are shown in *C* and *D*. MEGJ resistance is maintained at 900 MΩ with restricted diffusion between the projection and bulk EC. 10% of IP_3Rs are concentrated in the MP compartment.

depolarization transmitted through MEGJs to EC. Large increases in the gap junction permeability (~10^2-fold; $R_{gj} = 9$ MΩ), and maximum IP_3R current (~10^3-fold) in the single EC compartment model could compensate partially for the absence of MPs (Fig. 6*A* and *B*, dotted lines). From the results, it is evident that the presence of MPs facilitates the production of a hyperpolarizing feedback from EC to SMC following SMC stimulation.

IP_3 *vs.* Ca^{2+} signalling

Figure 7 examines the relative contributions of IP_3 and Ca^{2+} diffusion from stimulated SMC to EC to the generation of MP Ca^{2+} transients and the myoendothelial feedback. Average Ca^{2+} from MP in the 2D FEM model after SMC stimulation is plotted for different MEGJ resistances before (Fig. 7*A*) and after (Fig. 7*B*) blockade of intercellular IP_3 diffusion. Under control R_{gj} (900 MΩ as estimated by Yamamoto *et al.* 2001), IP_3 diffusion appears to be the major signalling molecule (Fig. 7*A*, continuous line), as the Ca^{2+} transient achieved by intercellular Ca^{2+} diffusion during IP_3 blockade (Fig. 7*B*, continuous line) is insignificant. In contrast, blocking Ca^{2+} diffusion did not cause a significant change in the MP Ca^{2+} transient (Fig. 7*B*, inset, dashed line *vs.* continuous line). Along with the Ca^{2+} transient, the feedback in SMC V_m is also abolished by blockade of IP_3 diffusion from SMC to EC (Fig. 7*C*, continuous *vs.* dashed lines). At low R_{gj} values (250 MΩ > R_{gj} > 50 MΩ, based on 70 MΩ from Sandow & Hill, 2000), The Ca^{2+} transient arising purely

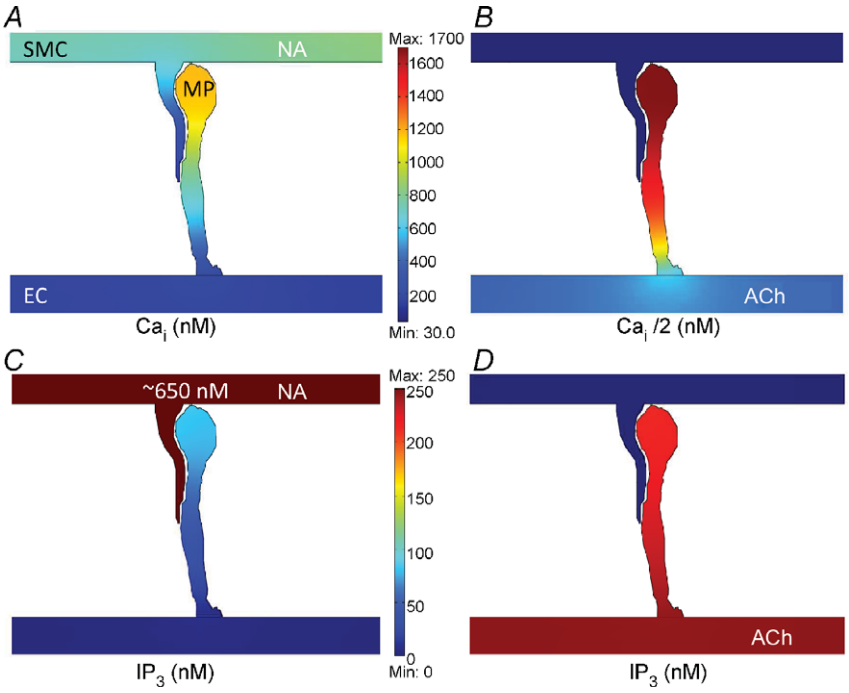

Figure 4.
2D FEM model results for NA stimulation of SMC (*A*, *C*) and ACh stimulation of EC (*B*, *D*). Predicted Ca^{2+} concentration inside the MP after NA stimulation of SMC (*A*) and bulk EC stimulation with ACh (*B*). The corresponding IP_3 transients in the MP for SMC and EC stimulation are shown in *C* and *D*, respectively. Ca^{2+} and IP_3 concentration profiles are shown 7.5 s after 1 μM NA stimulation of SMC and 2 s after ACh stimulation of EC, respectively.

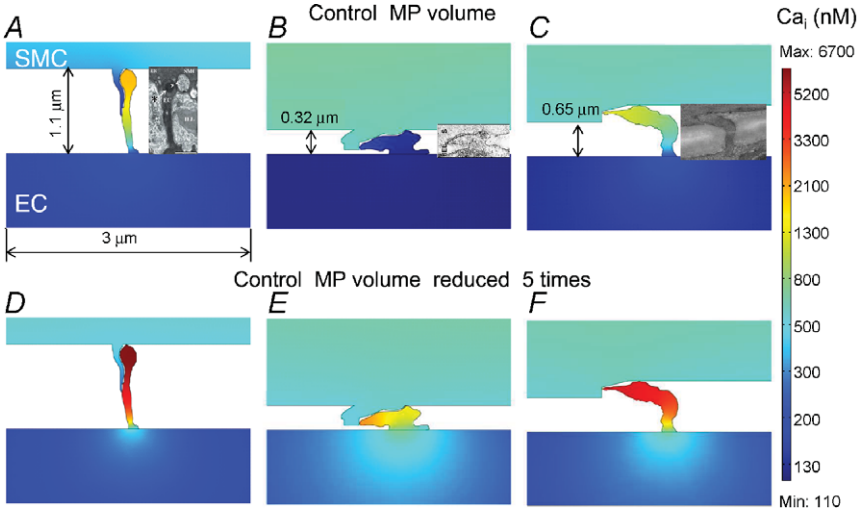

Figure 5.
Predicted Ca^{2+} concentration inside the MP after NA stimulation of SMC for different MP geometries: (*A*–*C*) control MP volume and shape, (*D*–*F*) MP volume reduced five-fold. Insets in (*A*–*C*) show the original electron microscopy images of the projections reproduced with permission from John Wiley and Sons, and The American Physiological Society (Heberlein *et al.* 2009; Sandow *et al.* 2009*b*; Tran *et al.* 2012).

from diffusion of Ca^{2+} (Fig. 7*B*) becomes significant and might cause a minor feedback. In general, the predicted Ca^{2+} transient in MP increases with decrease in R_{gj} and is mediated mainly by IP_3 rather than Ca^{2+} diffusion.

Effect of IK_{Ca} distribution

Experimental studies suggest that the quantity of IK_{Ca} channels in MPs is likely to vary between vascular beds and vessel types (Crane *et al.* 2003; Sandow *et al.* 2006; Dora *et al.* 2008; Ledoux *et al.* 2008*a*; Tran *et al.* 2012). Figure 8 shows the effect of varying IK_{Ca} distribution between MP and bulk EC on myoendothelial feedback in the compartmental model. The myoendothelial feedback after SMC stimulation increases with increased localization of IK_{Ca} channels in the MP (Fig. 8*A*), although the amount of IK_{Ca} channels in the MP does not affect the Ca^{2+} transient in the MP (Fig. 8*B*). The maximum feedback is achieved under control conditions with 100% IK_{Ca} channels present in the MP (Fig. 8*A*, continuous line). With uniform distribution of IK_{Ca} channels (Fig. 8*A*, dashed line), the model loses its ability to generate feedback and resembles the output of the model with no MP (Fig. 6*A*, dashed line).

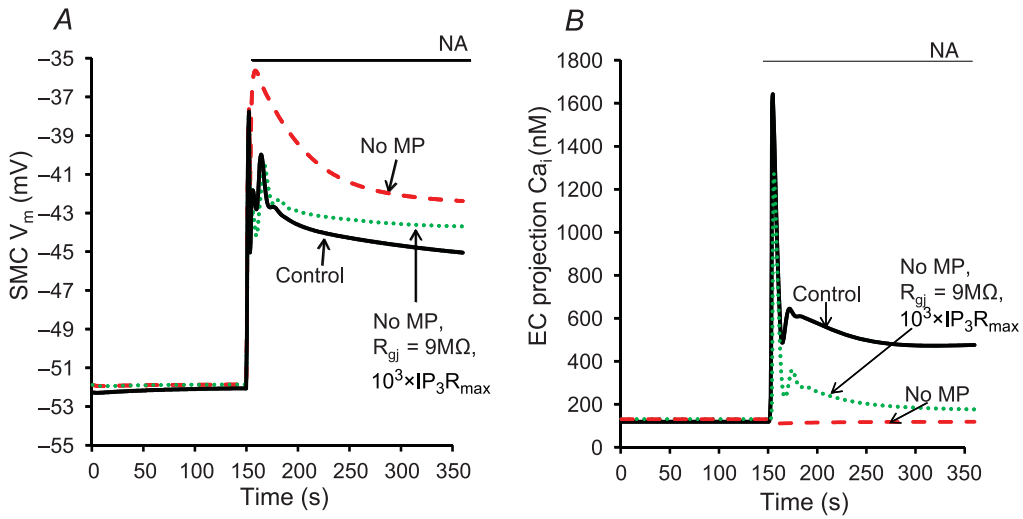

Figure 6.
SMC V_m (*A*) and EC MP Ca^{2+} (*B*) under three scenarios: no MP (dashed lines), control (continuous lines), and no MP with MEGJ resistance reduced from control 900 MΩ to 9 MΩ and the maximum IP_3R current increased 10^3-fold (dotted lines).

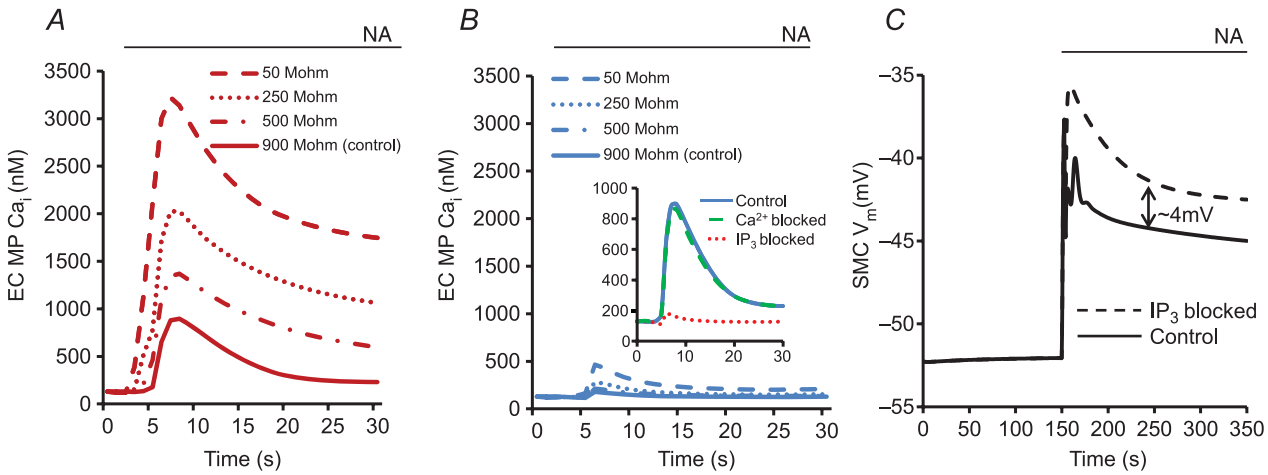

Figure 7.
Ca^{2+} transients in the MP after NA stimulation of SMC in the 2D FEM model under control conditions (*A*) and with IP_3 diffusion across MEGJs blocked (*B*), for different MEGJ resistances. The variation in R_{gj} is based on resistances estimated in experimental studies (Sandow & Hill, 2000; Yamamoto *et al.* 2001). *C*, SMC V_m under control conditions (continuous line) and with IP_3 diffusion from SMC to EC blocked in the compartmental model after NA stimulation of SMC. The arrow line (↕) shows the magnitude of the feedback mediated by the IP_3 diffusion.

Effect of R_{gj}

Values for the myoendothelial R_{gj} reported in the literature vary significantly. A lower value of 70 MΩ has been reported based on morphological observations. A higher value of 900 MΩ presents perhaps a better estimate as it was derived from electrical measurements (Sandow & Hill, 2000; Yamamoto *et al.* 2001; de Wit & Griffith, 2010). The effect of varying R_{gj} on the feedback is shown in more detail in Fig. 9. In all simulations, both IP_3 and Ca^{2+} coupling are present and the permeability of MEGJs to IP_3 and Ca^{2+} is inversely proportional to the assumed MEGJ resistance. Consistent with Fig. 7*A*, reduction of R_{gj} enhances the feedback in SMC V_m (Fig. 9*A*) and SMC Ca^{2+} (Fig. 9*B*). For low values of MEGJ resistances (<250 MΩ), IP_3 diffusion from SMC induces large Ca^{2+} responses in MP (Fig. 7*A*) and hyperpolarizing current from IK_{Ca} channels can overcome NA-induced SMC depolarization (Fig. 9*A*). This non-physiological response suggests that the combination of high IP_3R density in MP and low R_{gj} are not physiological. The magnitude of the feedback in SMC V_m and SMC Ca^{2+} *vs.* R_{gj} is shown in Fig. 9*C* and *D*. The feedbacks are calculated as the difference between SMC V_m (or Ca^{2+}) in the model with given R_{gj} and SMC V_m (or Ca^{2+}) in the model with no MP after 200 s of NA stimulation of SMC. The simulations without MP (and $R_{gj} = 900$ MΩ) are taken as the reference because no feedback response is generated in this scenario.

Effect of IP_3Rs

Immunohistochemical labelling techniques report a significant localization of IP_3Rs in the MPs, but their density and activation characteristics remain unclear and it is likely that they vary across different vascular beds (Isakson, 2008; Ledoux *et al.* 2008*a*; Ledoux J, 2008*b*; Sandow *et al.* 2009*b*). Figure 10 shows the predicted magnitude of the myoendothelial feedback as a function of IP_3R distribution. In these simulations, the IP_3R current was calculated according to eqn (4), which includes only IP_3-dependent (but not Ca^{2+}-dependent) activation. Greater feedback is achieved with higher IP_3R density in the MP and around 6 mV of hyperpolarizing feedback can be achieved with 30% IP_3R localization in MP (Fig. 10*C*, long dashed line). Under control conditions (10% IP_3Rs in MP), the maximum feedback achieved is around 3 mV (Fig. 9*A*, continuous *vs.* dashed lines) under the assumed parameter values.

Figure 11 examines whether the incorporation of Ca^{2+}-dependent activation of IP_3Rs and presence of basal IP_3 can increase the role of intercellular Ca^{2+} diffusion in the feedback response. In these simulations, the IP_3R current was calculated according to eqn (5), which includes both IP_3- and Ca^{2+}-dependent activations. SMC V_m at rest and following NA stimulation (1 μM) and is plotted as a function of basal IP_3 concentration in EC (i.e. EC prestimulation). Simulations are repeated after blocking Ca^{2+} diffusion (dashed line), blocking IP_3 diffusion (dotted line) and blocking both Ca^{2+} and IP3 diffusion (dashed-dotted line) between bulk EC and MP. The difference between the dashed-dotted and continuous lines is the amount of feedback. Simulations are performed for two different sensitivities of IP_3R activation to Ca^{2+} (i.e. K_{d_act}).

A first observation is that for both K_{d_act} values (Fig. 11*A* and *B*) SMC hyperpolarization when IP_3 exchange is present is the same as in control (dashed and continuous lines). Thus, IP_3 diffusion alone can produce maximum

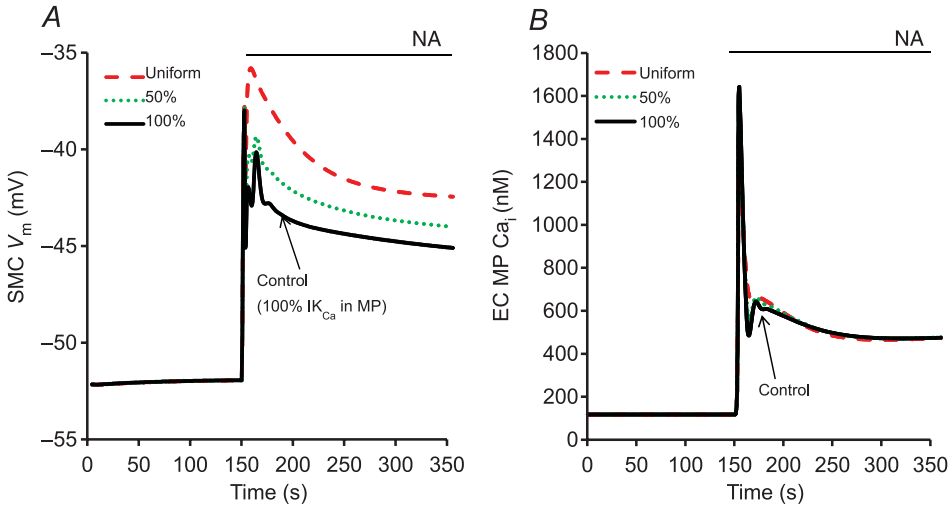

Figure 8.
Compartmental model results showing SMC V_m (*A*) and Ca^{2+} concentration in the EC MP (*B*) after stimulation with NA under different IK_{Ca} distribution in EC. Uniform IK_{Ca} (dashed lines), 50% of IK_{Ca} channels in MP (dotted lines), and all IK_{Ca} channels in MP (continuous lines).

feedback response regardless of the contribution or not from Ca^{2+}. With a low Ca^{2+}-dependent IP_3R activation parameter ($K_{d\_act} = 130$ nM), Ca^{2+} diffusion alone does not generate significant feedback at any basal IP_3 in EC (Fig. 11*A*, dotted *vs.* dashed-dotted line). IP_3 diffusion generates feedback of a few millivolts at low basal IP_3, and larger feedback at intermediate concentrations of basal IP_3 (~25 nM; Fig. 11*A*, dashed *vs.* dashed-dotted line). Ca^{2+} diffusion has a small synergistic effect with IP_3 diffusion at low basal IP_3, but it has no effect at intermediate and high basal IP_3 (Fig. 11*A*, dashed *vs.* continuous line). High basal IP_3 (>35 nM) activates EC independently from SMC and limits the feedback response.

With a high Ca^{2+}-dependent activation parameter ($K_{d\_act} = 350$ nM), Ca^{2+} diffusion alone could generate significant feedback in the presence of appropriate basal IP_3 in EC (Fig. 11*B*, dotted *vs.* dashed-dotted line). EC prestimulation with basal IP_3 in the range of 30–45 nM partially activates IP_3Rs and elevates resting Ca^{2+} near K_{d_act}. At this point IP_3Rs in MP are sensitized to small Ca^{2+} fluxes from SMC, and significant myoendothelial feedback can be mediated without IP_3 coupling. IP_3 diffusion generates weak feedback at low basal IP_3, and large feedback at intermediate concentrations of basal IP_3 (<45 nM; Fig. 11*B*, dashed *vs.* dashed-dotted line). In the presence of IP_3 coupling, Ca^{2+} diffusion has little or no effect on the feedback (Fig. 11*A*, dashed *vs.* continuous line). In general, basal IP_3 can sensitize EC to IP_3 and Ca^{2+} fluxes from SMC. However, IP_3 diffusion can initiate a significant feedback response under many scenarios of parameter values and conditions, while Ca^{2+} diffusion is required only when IP_3 diffusion is blocked and its potential for feedback is conditional on an appropriate value for the sensitivity of the IP_3R to Ca^{2+} and the existence of basal IP_3 levels within a narrow concentration window.

Discussion

The primary aim of this study was to understand the role of MPs in myoendothelial signalling. Using the proposed models, we examined the effect of MPs on the intracellular Ca^{2+} gradients in EC during SMC stimulation

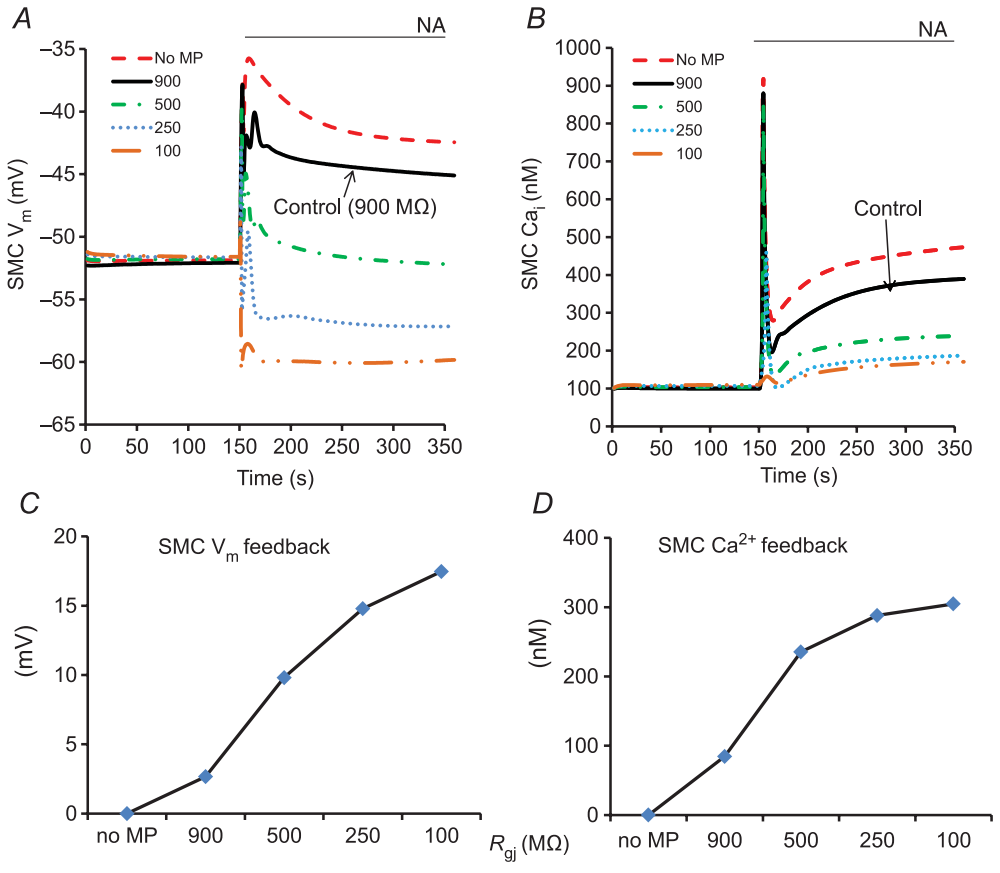

Figure 9.
Compartmental model predictions of SMC V_m (*A*) and SMC Ca^{2+} transients (*B*) after SMC stimulation with NA for different R_{gj} values as shown in panel keys. The magnitude of the feedback in SMC V_m (*C*) and Ca^{2+} (*D*) is calculated at the end of simulation as a difference between the model with given R_{gj} and the 'no MP' model(dashed lines).

and the resulting NO-independent vasodilatory feedback response from EC to SMC. Simulations show the effect of MP geometry, MEGJ coupling, R_{gj}, IK_{Ca} distribution, IP_3R density and activation parameters, and basal IP_3.

EC-to-SMC communication

Endothelial control of vascular tone is attributed to an increase in EC Ca^{2+} followed by the activation of Ca^{2+}-dependent vasodilatory pathways such as EDRF, prostacyclin (PGI_2) and EDHF (Dora *et al.* 1997; Sandow, 2004; Feletou & Vanhoutte, 2006) among others. Both the compartmental and 2D FEM models could simulate SMC relaxation induced by ACh stimulation of EC and mediated by EDHF, consistent with experimental data and the previous EC–SMC model (Dora *et al.* 1997; Oishi *et al.* 2001; Schuster *et al.* 2001; Lamboley *et al.* 2005; Kapela *et al.* 2009). ACh stimulation increased IP_3 and Ca^{2+} in EC bulk and MP (Fig. 4*A* and *B*), leading to activation of SK_{Ca} and IK_{Ca} channels. The hyperpolarizing current from SK_{Ca} and IK_{Ca} channels was transmitted by the MEGJs to SMC and reduced SMC Ca^{2+}. Presence of MP did not compromise EDHF, and EC MP was effectively isopotential with EC bulk.

SMC-to-EC communication

An increasing amount of evidence shows the existence of local EC Ca^{2+} events such as 'pulsars' and 'wavelets' in and around EC MPs following SMC stimulation without significant global spread (Kansui *et al.* 2008; Ledoux *et al.* 2008*b*; Tran *et al.* 2012). Similarly, following SMC stimulation in the models, the IP_3 and Ca^{2+} increase in EC was confined to the MPs and its spread into the bulk EC was rather limited (Fig. 3*A*, 4*A* and *C*). The amplitude of Ca^{2+} transients in the MPs depended upon the size and shape of the projection (Fig. 5) and the area available for diffusion of ions into the bulk EC. Theoretical estimations suggest that passive diffusion of Ca^{2+} and/or IP_3 into EC is insufficient for a global Ca^{2+} mobilization (Nagaraja

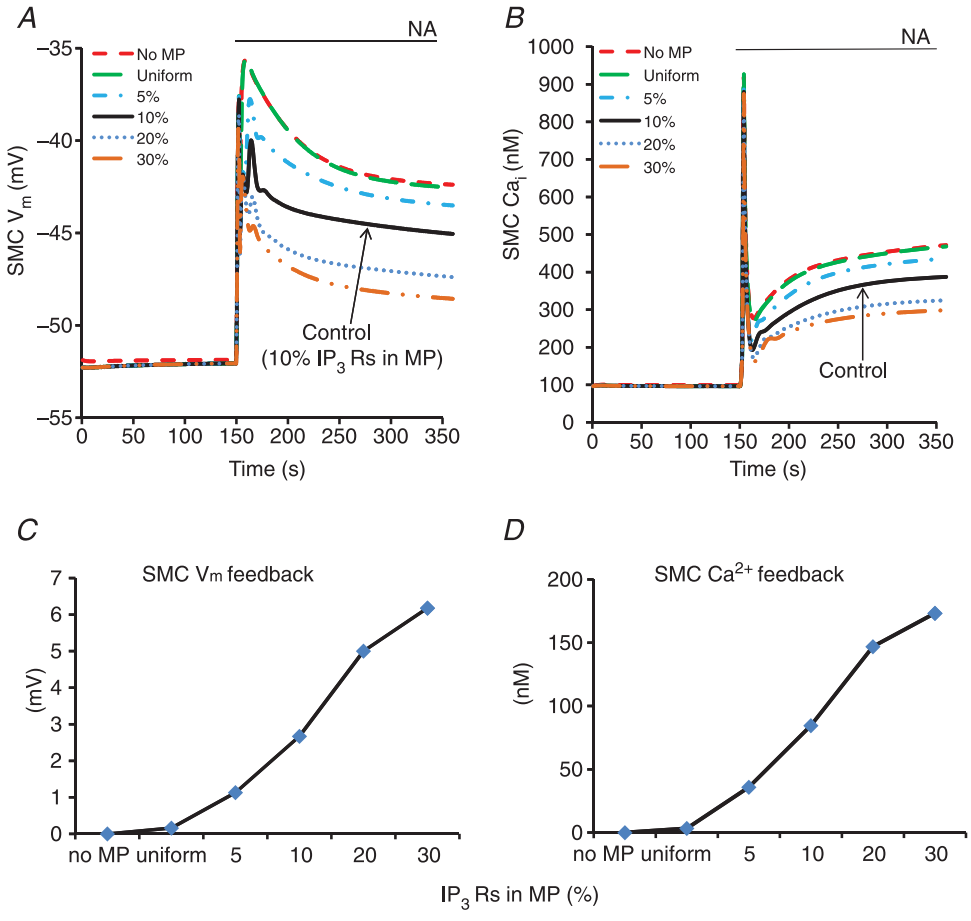

Figure 10.
Compartmental model predictions of SMC V_m (*A*) and SMC Ca^{2+} transients (*B*) for different IP_3R densities inside the MP as shown in panel keys. The magnitude of the feedback in SMC V_m (*C*) and SMC Ca^{2+} (*D*) is calculated at the end of simulation as a difference between the model with given IP_3R distribution and the 'no MP' model(dashed lines).

et al. 2012). The small size of MP as compared to the bulk cytosol and restricted diffusivity from MP into bulk EC allows for significant accumulation of IP_3 and/or Ca^{2+} following SMC stimulation. RyRs and/or IP_3Rs like those found in MPs can further amplify the weak fluxes of Ca^{2+} and IP_3 to induce local Ca^{2+} transients and EC hyperpolarization (Isakson, 2008; Ledoux *et al.* 2008*a*).

In earlier studies, a global Ca^{2+} increase in EC after SMC stimulation has also been reported (Dora *et al.* 1997; Yashiro & Duling, 2000; Schuster *et al.* 2001; Tuttle & Falcone, 2001; Jackson *et al.* 2008). The reason for this discrepancy may be attributed to differences in the experimental techniques employed. Our results suggest that if a global response does happen, a mechanism to amplify the small local events is necessary. The presence of a currently unidentified regeneration mechanism cannot be excluded. In fact, in a recent theoretical study Brasen *et al.* (2012)showed that a Ca^{2+} transient in the MP, induced by IP_3 elevation in SMC, could subsequently spread into the entire EC as a Ca^{2+} wave through CICR in IP_3Rs. CICR was possible because of sensitization of EC bulk with basal IP_3 levels (0.1 μM) and not because of IP_3 spread from the SMC and MP to EC bulk. This study did not account for membrane electrophysiology. In our model, sub-threshold levels of IP_3 enhanced significantly the feedback without generating global EC Ca^{2+}, while further elevation of basal IP_3 hyperpolarized resting V_m (Fig. 11). These results show that fine tuning of the system's excitability may allow facilitation of Ca^{2+} spread, but at least in our model, NA-induced Ca^{2+} transients are more likely to have limited spread, in agreement with recent experimental studies (Kansui *et al.* 2008; Ledoux *et al.* 2008*b*; Tran *et al.* 2012).

MPs amplify feedback

In the model, the local Ca^{2+} transients and IK_{Ca} channels in the EC MPs generated a hyperpolarizing feedback in SMC of around 3 mV (Fig. 6*A*, continuous line). In simulations with no diffusional resistance between the MPs and bulk EC and thus effectively no MPs, the feedback was lost (Fig. 6*A*, dashed line), in spite of the IP_3R and IK_{Ca} localization still present near the MEGJs. In the absence of a restricted space like the MPs, the IP_3 and Ca^{2+} entering the MPs from the stimulated SMC rapidly diffused into the entire endothelial cell and failed to produce a local or global Ca^{2+} increase (Fig. 6*B*, dashed line), because of dilution in large cytosolic volume, Ca^{2+} sequestration and buffering, and IP_3 degradation by one to five phosphatases present in the cytosol. Increasing the

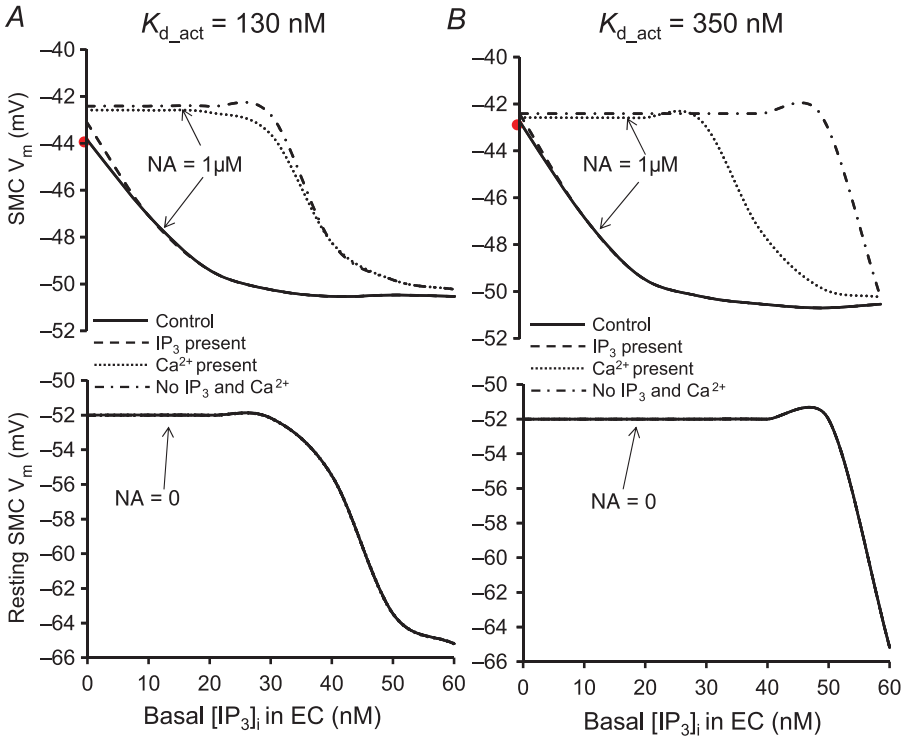

Figure 11.
Compartmental model predictions of SMC V_m after 200 s of NA stimulation and at rest (NA = 0) for different basal IP_3 concentrations in the EC, with control MEGJ coupling (continuous lines), IP_3 diffusion alone (Ca^{2+} diffusion blocked) (dashed lines), Ca^{2+} diffusion alone (IP_3 diffusion blocked) (dotted lines), and no IP_3 or Ca^{2+} diffusion (dashed-dotted lines). *A*, simulations with low EC IP_3R K_{d_act} = 130 nM. *B,* simulations with high EC IP_3R K_{d_act} = 350 nM.

gap junction permeability 10^2-fold and maximum IP_3R current 10^3-fold failed to fully compensate the lack of MPs (Fig. 6*A*, continuous *vs.* dotted lines). Thus, it appears that in conjunction with the localization of IK_{Ca} and IP_3Rs, the presence of a restricted space like a MP within the EC is essential for Ca^{2+} mobilization in the EC and facilitation of feedback following SMC stimulation. It is important to note here that the differences in Ca^{2+} and IP_3 concentration between the MPs and bulk EC, as well as the spread of MP Ca^{2+} into the bulk EC, will depend on the relative size, surface area and volume of the MP with respect to the bulk of EC (Fig. 5).

Ca^{2+} accumulation may be further enhanced by the close proximity of ER and mitochondria to the plasma membrane. The presence of organelles at the base of the MP, for example, will restrict diffusion to the bulk of EC, enabling significant Ca^{2+} transients in the vicinity of MP which could activate components that are not necessarily placed within the MP. Thus, in general, small spaces restricted by MP and/or subcellular structures seem to be imperative for amplification of SMC initiated signals causing local Ca^{2+} events and the experimentally observed feedback of a few millivolts (Tran *et al.* 2012). The inhibition of SK_{Ca}/IK_{Ca} channels enhanced NA-induced depolarization by ∼3.5 mV and was associated with about 10% smaller diameter of NA-constricted vessels (Tran *et al.* 2012). Since the resistance to flow is inversely proportional to diameter to the fourth power (i.e. Poiseuille equation), this change corresponds to a very significant (more than 50%) increase in resistance.

MEGJs and R_{gj}

MEGJs are the primary NO-independent pathway for transfer of agonist induced EC hyperpolarization to the SMC (Sokoya *et al.* 2006; Isakson *et al.* 2007; Kansui *et al.* 2008). Their presence has been documented in various vascular beds (Figueroa *et al.* 2004), including rat mesenteric arteries (Hill *et al.* 2000; Sandow & Hill, 2000), using direct as well as indirect methods like electron microscopy and dye coupling between two cells (Little *et al.* 1995; Beny, 1997). MEGJs also transmit V_m changes from SMC to EC, although differences in input resistances of endothelial and smooth muscle layers can cause asymmetric ME responses (Emerson & Segal, 2000; Diep *et al.* 2005). Furthermore, the highest occurrences of MEGJs have been observed in small arteries and arterioles coincidental with a high number of MPs and high EDHF activity (Hwa *et al.* 1994; Sandow *et al.* 2009*a*). Myoendothelial signalling is highly diminished or even abolished in the presence of gap junction blockers like 18-glycyrrhetinic acid (18-GA) and carbenoxolone (Hill *et al.* 2000; Goto *et al.* 2002; Hill *et al.* 2002; Dora *et al.* 2003; Sandow *et al.* 2004; Mather *et al.* 2005; Sokoya *et al.* 2006; Dora *et al.* 2008), but not after eNOS inhibition (Nausch *et al.* 2012). Some vessels may lack MEGJs and functional ME coupling (Sandow *et al.* 2002; Siegl *et al.* 2005). Gap junctions are believed to be non-selective in nature, with similar permeabilities for small ions (Christ *et al.* 1996; Brink *et al.* 2000). Experimentally estimated values of R_{gj} are spread over a large range, 70–900 MΩ, depending on the particular tissue and experimental conditions and the type of cells being examined (Sandow & Hill, 2000; Yamamoto *et al.* 2001; de Wit & Griffith, 2010). In the simulations, a decrease in R_{gj} is associated with increased permeability of MEGJs to Ca^{2+} and IP_3 and and increase in Ca^{2+} transients in the EC MP (Fig. 7*A*). This in turn led to higher feedback in terms of SMC Ca^{2+} and SMC V_m (Fig. 9). Under control density of IP_3Rs and IK_{Ca} channels in MP and with Ca^{2+} and IP_3 diffusion through MEGJs, resistances below 500 MΩ caused Ca^{2+} transients in the MP to be high enough to counteract the SMC depolarization to NA stimulation (Fig. 9*A*). This suggests lower IP_3R density in MPs and/or higher R_{gj}.

Localization of IP_3Rs

IP_3R localization will be an important determinant of amplitude of Ca^{2+} transients in the MP (Lamboley *et al.* 2005; Isakson, 2008; Sandow *et al.* 2009*b*). While a significant number of IP_3R clusters seem to be present along the projections (Ledoux *et al.* 2008*a*; Sandow *et al.* 2009*b*), IP_3Rs in the rest of the EC are primarily responsible for experimentally observed global Ca^{2+} increase in EC after ACh stimulation, which is most likely initiated from the luminal side of the EC, opposite to the location of MPs. Results from the compartmental model showed an increase in feedback in terms of SMC V_m and SMC Ca^{2+} with increase in IP_3R localization in the MP, predicting a hyperpolarizing feedback of up to 6 mV with 30% IP_3R localization (Fig. 10*C*). ER is a dynamic and flexible structure spread throughout the EC and undergoing constant change. ER provides a single continuous space for the movement of Ca^{2+} ions and can direct Ca^{2+} movement in the cell by concentrating IP_3Rs in a particular cellular region (Diambra & Marchant, 2009; Taylor *et al.* 2009). Perhaps, for this reason, ER localizes at the base and inside of some projections so as to increase the density of IP_3R in the projection to form a local regulating module to enhance the feedback of EC to SMC. With better quantification of the relative densities of these receptors in the MP as compared to the whole EC, we can obtain a better estimate of the feedback capacity of MPs.

Localization of IK_{Ca} channels

The co-localization of IK_{Ca} channels close to IP_3Rs is crucial for facilitation of feedback by MPs. Experimental studies in some tissues show a spatial separation of the two types of K_{Ca} channels expressed in the ECs (Crane

et al. 2003; Sandow *et al.* 2006; Dora *et al.* 2008). In rat mesenteric arteries, IK_{Ca} channels are predominantly expressed in and around the MPs (Dora *et al.* 2008; Ledoux *et al.* 2008*a*; Sandow *et al.* 2009*b*), while SK_{Ca} channels are mostly confined to the bulk of EC near EC–EC tight junctions (Crane *et al.* 2003; Sandow *et al.* 2006). MPs contain most of the IK_{Ca} channels that along with SK_{Ca} channels are responsible for EC hyperpolarization during EC stimulation (Doughty *et al.* 1999; Crane *et al.* 2003; Tran *et al.* 2012). This segregation of IK_{Ca} and SK_{Ca} channels might be a way to separate the respective roles of the very closely related and similarly activated K_{Ca} channels. Because of their localization in the MP, IK_{Ca} channels might be engaged in a local feedback mechanism through MP Ca^{2+}. Model predictions showed that, during SMC stimulation, the concentration of Ca^{2+} in the MPs increased as high as the global Ca^{2+} concentration in EC during ACh (a potent vasodilator) stimulation of EC (Fig. 3*A vs. B*) Therefore, this unique orientation of IK_{Ca} channels near the *local* Ca^{2+} transients might dismiss the need of a *global* response. This is also reflected in the fact that for the same Ca^{2+} transient in the MP (Fig. 8*B*), the feedback generated with the control model (100% IK_{Ca} channels localized to MP) was lost with uniform distribution of these channels (Fig. 8*A*, continuous *vs.* dashed lines). The feedback progressively decreased with a decrease in the number of IK_{Ca} channels localized in the MP. For these simulations, R_{gj} and IP_3R density were maintained at their respective control values.

IP_3 diffusion

Experimental results suggest that Ca^{2+} mobilization in EC after SMC stimulation can be attributed mostly to diffusion of IP_3 rather than Ca^{2+} (Lamboley *et al.* 2005; Isakson *et al.* 2007; Tran *et al.* 2012). Vascular co-culture studies by Isakson *et al.* showed that IP_3R blockade in ECs inhibits Ca^{2+} flashes in ECs induced by agonist stimulation of BAPTA-loaded SMCs (Isakson *et al.* 2007; Isakson, 2008). A similar blocking of IP_3Rs in SMC following EC stimulation, however, did not alter SMC response due to lack of IP_3R localization on the SMC side of the myoendothelial junction and an abundance of IP_3 metabolizer 5-phosphatase (Isakson, 2008). Experiments on rat mesenteric arteries by Lamboley *et al.* (2005) showed that blocking of any component of the IP_3 signalling pathway (PLC inhibition in SMC, IP_3R blocking in EC) led to a severe reduction in Ca^{2+} transients in ECs following SMC stimulation. In a recent study in hamster vessels, Tran *et al.* (2012) showed that blockade of EC IP_3Rs inhibits feedback in SMC V_m (by ∼4 mV) during SMC stimulation with an IP_3 releasing vasoconstrictor (PE), as seen in our simulations (Fig. 7*C*, dashed line). A similar blockade of EC IP_3Rs did not alter SMC depolarization and constriction due to a non-IP_3 releasing voltage-dependent potassium channel (K_v) blocker, 4-aminopyridine (4-AP) (Tran *et al.* 2012). In agreement with the experimental observations, the 2D FEM model results under control (Fig. 7*A*) and blocked IP_3 diffusion (Fig. 7*B*) conditions for different R_{gj} values predicted a significant reduction (∼4 times) in Ca^{2+} transients by blockade of IP_3 diffusion from SMC to EC, which suggests that the majority of Ca^{2+} transient can be attributed to the diffusion of IP_3 and not Ca^{2+}.

Ca^{2+} diffusion

Earlier studies suggested that Ca^{2+} mobilization in EC after SMC stimulation is mediated by diffusion of Ca^{2+} ions (Dora *et al.* 1997; Schuster *et al.* 2001), but this hypothesis has not been supported experimentally. In our control model, blocking of Ca^{2+} diffusion from SMC to EC did not alter the MP Ca^{2+} transient (Fig. 7*B*, inset). Ca^{2+} diffusion alone appears to produce some Ca^{2+} increase in the MP only at low values of R_{gj} (<50 MΩ; Fig. 7*B*, dashed line). In the model with Ca^{2+}- and IP_3-activated IP_3Rs (eqn (5)), Ca^{2+} diffusion can activate IP_3Rs in synergy with IP_3 diffusion (Fig. 11*A*) or in the presence of basal IP_3 levels in the EC (Fig. 11*B*). The basal concentration of IP_3 needs to be adequate enough to sensitize IP_3R in ECs to weak Ca^{2+} flux, but at the same time it should not increase the resting EC MP Ca^{2+} levels and induce CICR prior to SMC stimulation (Nagaraja *et al.* 2012). Hence, there appears to be a narrow window of basal IP_3 levels for which Ca^{2+} might be able to contribute to the feedback response. The adequacy of basal IP_3 will be influenced by the degree of IP_3R localization and the half-maximum activation concentration (K_{d_act}) of both IP_3 and Ca^{2+} for the IP_3R. So far, there is no direct evidence for simultaneous existence of all these conditions in the EC. In our model, for a limited set of parameters (K_{d_act} = 350 nM; basal IP_3 between 30–50 nM), Ca^{2+} diffusion could produce a hyperpolarizing feedback of up to 6 mV for control values of R_{gj}, IP_3R and IK_{Ca} localization (Fig. 11*B*, dotted line). However, for this high value of K_{d_act}, the IP_3R activation and feedback (∼0.5 mV) are much smaller in the absence of basal IP_3 compared to the control model.

Limitations

A number of parameter values have not been accurately quantified. In this study, we try to remain consistent with our previous EC–SMC model with respect to parameter values and whole cell currents (i.e. most parameters were derived in this earlier study from rat mesenteric artery data). The important deviations were the maximum IP_3R current and permeability of MEGJs to IP_3. These parameters had been increased 10^3- and 10^2-fold in the

earlier EC–SMC model to compensate for the lack of MPs and to allow for myoendothelial feedback. The models' behaviour is sensitive to a number of tissue specific parameters such as channel conductances, myoendothelial IP_3 permeability, dimension and number of MPs, localization and density of IP_3Rs, SK_{Ca}/IK_{Ca} channels, and MEGJs inside the MPs. This limitation was partially addressed through parametric studies that examine the effect of parameter uncertainty on the models' predictions.

The compartmental model captures well the electrical aspects of the myoendothelial coupling, but cannot accurately simulate subcellular concentration gradients and exchange of species. The 2D model is better suited to simulate Ca^{2+} transients in the vicinity of MPs and to account for the MP geometry and the spatial distribution of channels and receptors. The 2D model is limited, however, by the absence of quantification for the spatial distribution of these important cellular components. The integrated CICR mechanism is not sufficient to facilitate significant Ca^{2+} spread in the models. Other regenerative mechanisms might also exist that could enhance Ca^{2+} and IP_3 diffusion. For example, IP_3 generation by Ca^{2+} (via Ca^{2+}-dependent PLC) in ECs might lead to global Ca^{2+} mobilization in the EC. At this point, however, such mechanisms have not been established experimentally.

By assuming only a single EC and SMC pair, the model simulates an average behaviour spatiotemporally. That is, every EC in the vessel is hyperpolarized to the same level for the entire duration. In reality, only a small percentage of ECs will exhibit NA-induced MP Ca^{2+} wavelets at any given time (Tran *et al.* 2012). Depending on the number of active sites, the duration and frequency of the events, the IK_{Ca} current required per MP must be stronger to compensate for current loss to other ECs. The model does not account for the transient/stochastic behaviour of Ca^{2+} mobilization seen in the experimental studies. Figures 8–10 show, however, that a single MP is capable of generating much stronger hyperpolarizing currents.

Conclusions

The models developed in this study present a first attempt to capture the role of MPs in the myoendothelial feedback. The models predict that even in the absence of NO signalling pathway, EC is able to generate the few-millivolt (i.e. 2–3 mV) feedback observed experimentally, thanks to the presence of signalling microdomains composed of MPs with small cytosolic volume, restricted permeability to bulk EC, and localized IP_3Rs and IK_{Ca} channels. In agreement with recent experimental evidence (Tran *et al.* 2012) the model predicts that IP_3, rather than Ca^{2+}, diffusion from SMC to EC is the mechanism responsible for the Ca^{2+} transients in the EC MPs after SMC agonist stimulation. These Ca^{2+} transients are localized primarily within the MPs, with limited spread into EC bulk. A global spread would thus require the presence of a regeneration mechanism in the bulk of EC. The amount of feedback depends on various parameters, but simulations suggest that MPs are required for a significant feedback. Thus, our results highlight the importance of MPs in myoendothelial communication by amplifying local Ca^{2+} increase and facilitating the generation of feedback response to SMC constriction.

References

Allbritton NL, Meyer T & Stryer L (1992). Range of messenger action of calcium ion and inositol 1,4,5-trisphosphate. *Science* **258**, 1812–1815.

Atri A, Amundson J, Clapham D & Sneyd J (1993). A single-pool model for intracellular calcium oscillations and waves in the *Xenopus laevis* oocyte. *Biophys J* **65**, 1727–1739.

Beny J (1997). Electrical coupling between smooth muscle cells and endothelial cells in pig coronary arteries. *Pflugers Arch* **433**, 364–367.

Brasen JC, Jacobsen JC & Holstein-Rathlou NH (2012). The nanostructure of myoendothelial junctions contributes to signal rectification between endothelial and vascular smooth muscle cells. *PLoS One* **7**, e33632.

Brink PR, Ricotta J & Christ GJ (2000). Biophysical characteristics of gap junctions in vascular wall cells: implications for vascular biology and disease. *Braz J Med Biol Res* **33**, 415–422.

Bychkov R, Burnham MP, Richards GR, Edwards G, Weston AH, Feletou M & Vanhoutte PM (2002). Characterization of a charybdotoxin-sensitive intermediate conductance Ca^{2+}-activated K^+ channel in porcine coronary endothelium: relevance to EDHF. *Br J Pharmacol* **137**, 1346–1354.

Christ GJ, Spray DC, el-Sabban M, Moore LK & Brink PR (1996). Gap junctions in vascular tissues. Evaluating the role of intercellular communication in the modulation of vasomotor tone. *Circ Res* **79**, 631–646.

Crane GJ, Gallagher N, Dora KA & Garland CJ (2003). Small- and intermediate-conductance calcium-activated K^+ channels provide different facets of endothelium-dependent hyperpolarization in rat mesenteric artery. *J Physiol* **553**, 183–189.

de Wit C & Griffith TM (2010). Connexins and gap junctions in the EDHF phenomenon and conducted vasomotor responses. *Pflugers Arch* **459**, 897–914.

Diambra L & Marchant JS (2009). Localization and socialization: experimental insights into the functional architecture of IP_3 receptors. *Chaos* **19**, 037103.

Diep HK, Vigmond EJ, Segal SS & Welsh DG (2005). Defining electrical communication in skeletal muscle resistance arteries: a computational approach. *J Physiol* **568**, 267–281.

Dora KA, Doyle MP & Duling BR (1997). Elevation of intracellular calcium in smooth muscle causes endothelial cell generation of NO in arterioles. *Proc Natl Acad Sci U S A* **94**, 6529–6534.

Dora KA, Gallagher NT, McNeish A & Garland CJ (2008). Modulation of endothelial cell KCa3.1 channels during endothelium-derived hyperpolarizing factor signaling in mesenteric resistance arteries. *Circ Res* **102**, 1247–1255.

Dora KA, Sandow SL, Gallagher NT, Takano H, Rummery NM, Hill CE & Garland CJ (2003). Myoendothelial gap junctions may provide the pathway for EDHF in mouse mesenteric artery. *J Vasc Res* **40**, 480–490.

Doughty JM, Plane F & Langton PD (1999). Charybdotoxin and apamin block EDHF in rat mesenteric artery if selectively applied to the endothelium. *Am J Physiol Heart Circ Physiol* **276**, H1107–H1112.

Emerson GG & Segal SS (2000). Electrical coupling between endothelial cells and smooth muscle cells in hamster feed arteries: role in vasomotor control. *Circ Res* **87**, 474–479.

Feletou M & Vanhoutte PM (2006). Endothelium-derived hyperpolarizing factor: where are we now? *Arterioscler Thromb Vasc Biol* **26**, 1215–1225.

Figueroa XF, Isakson BE & Duling BR (2004). Connexins: gaps in our knowledge of vascular function. *Physiology (Bethesda)* **19**, 277–284.

Finch EA, Turner TJ & Goldin SM (1991). Calcium as a coagonist of inositol 1,4,5-trisphosphate-induced calcium release. *Science* **252**, 443–446.

Garland CJ, Plane F, Kemp BK & Cocks TM (1995). Endothelium-dependent hyperpolarization: a role in the control of vascular tone. *Trends Pharmacol Sci* **16**, 23–30.

Goto K, Fujii K, Kansui Y, Abe I & Iida M (2002). Critical role of gap junctions in endothelium-dependent hyperpolarization in rat mesenteric arteries. *Clin Exp Pharmacol Physiol* **29**, 595–602.

Heberlein KR, Straub AC & Isakson BE (2009). The myoendothelial junction: breaking through the matrix? *Microcirculation* **16**, 307–322.

Hill CE, Hickey H & Sandow SL (2000). Role of gap junctions in acetylcholine-induced vasodilation of proximal and distal arteries of the rat mesentery. *J Auton Nerv Syst* **81**, 122–127.

Hill CE, Rummery N, Hickey H & Sandow SL (2002). Heterogeneity in the distribution of vascular gap junctions and connexins: implications for function. *Clin Exp Pharmacol Physiol* **29**, 620–625.

Hwa JJ, Ghibaudi L, Williams P & Chatterjee M (1994). Comparison of acetylcholine-dependent relaxation in large and small arteries of rat mesenteric vascular bed. *Am J Physiol Heart Circ Physiol* **266**, H952–H958.

Isakson BE (2008). Localized expression of an Ins(1,4,5)P_3 receptor at the myoendothelial junction selectively regulates heterocellular Ca^{2+} communication. *J Cell Sci* **121**, 3664–3673.

Isakson BE, Ramos SI & Duling BR (2007). Ca^{2+} and inositol 1,4,5-trisphosphate-mediated signaling across the myoendothelial junction. *Circ Res* **100**, 246–254.

Jackson WF, Boerman EM, Lange EJ, Lundback SS & Cohen KD (2008). Smooth muscle alpha1D-adrenoceptors mediate phenylephrine-induced vasoconstriction and increases in endothelial cell Ca^{2+} in hamster cremaster arterioles. *Br J Pharmacol* **155**, 514–524.

Jacobsen JC, Aalkjaer C, Nilsson H, Matchkov VV, Freiberg J & Holstein-Rathlou NH (2007). Activation of a cGMP-sensitive calcium-dependent chloride channel may cause transition from calcium waves to whole cell oscillations in smooth muscle cells. *Am J Physiol Heart Circ Physiol* **293**, H215–H228.

Kansui Y, Garland CJ & Dora KA (2008). Enhanced spontaneous Ca^{2+} events in endothelial cells reflect signalling through myoendothelial gap junctions in pressurized mesenteric arteries. *Cell Calcium* **44**, 135–146.

Kapela A, Bezerianos A & Tsoukias NM (2008). A mathematical model of Ca^{2+} dynamics in rat mesenteric smooth muscle cell: agonist and NO stimulation. *J Theor Biol* **253**, 238–260.

Kapela A, Bezerianos A & Tsoukias NM (2009). A mathematical model of vasoreactivity in rat mesenteric arterioles: I. Myoendothelial communication. *Microcirculation* **16**, 694–713.

Kapela A & Tsoukias NM (2011). Multiscale FEM modeling of vascular tone: from membrane currents to vessel mechanics. *IEEE Trans Biomed Eng* **58**, 3456–3459.

Kerr PM, Tam R, Ondrusova K, Mittal R, Narang D, Tran CH, Welsh DG & Plane F (2012). Endothelial feedback and the myoendothelial projection. *Microcirculation* **19**, 416–422.

Lamboley M, Pittet P, Koenigsberger M, Sauser R, Beny JL & Meister JJ (2005). Evidence for signaling via gap junctions from smooth muscle to endothelial cells in rat mesenteric arteries: possible implication of a second messenger. *Cell Calcium* **37**, 311–320.

Ledoux J, Boney AD, Hannah RM, Tallini YN, Kotlikoff MI & Nelson MT (2008*b*). Ca^{2+} pulsars: spatially restricted, IP_3R-mediated Ca2+ release important for endothelial function. *J Vasc Res* **45**(Suppl. 1), 102.

Ledoux J, Taylor MS, Bonev AD, Hannah RM, Solodushko V, Shui B, Tallini Y, Kotlikoff MI & Nelson MT (2008*a*). Functional architecture of inositol 1,4,5-trisphosphate signaling in restricted spaces of myoendothelial projections. *Proc Natl Acad Sci U S A* **105**, 9627–9632.

Little TL, Xia J & Duling BR (1995). Dye tracers define differential endothelial and smooth muscle coupling patterns within the arteriolar wall. *Circ Res* **76**, 498–504.

Luksha L, Agewall S & Kublickiene K (2009). Endothelium-derived hyperpolarizing factor in vascular physiology and cardiovascular disease. *Atherosclerosis* **202**, 330–344.

McNeish AJ, Sandow SL, Neylon CB, Chen MX, Dora KA & Garland CJ (2006). Evidence for involvement of both IKCa and SKCa channels in hyperpolarizing responses of the rat middle cerebral artery. *Stroke* **37**, 1277–1282.

Mather S, Dora KA, Sandow SL, Winter P & Garland CJ (2005). Rapid endothelial cell-selective loading of connexin 40 antibody blocks endothelium-derived hyperpolarizing factor dilation in rat small mesenteric arteries. *Circ Res* **97**, 399–407.

Moore DH & Ruska H (1957). The fine structure of capillaries and small arteries. *J Biophys Biochem Cytol* **3**, 457–462.

Nagaraja S, Kapela A & Tsoukias NM (2012). Intercellular communication in the vascular wall: a modeling perspective. *Microcirculation* **19**, 391–402.

Nausch LW, Bonev AD, Heppner TJ, Tallini Y, Kotlikoff MI & Nelson MT (2012). Sympathetic nerve stimulation induces local endothelial Ca^{2+} signals to oppose vasoconstriction of mouse mesenteric arteries. *Am J Physiol Heart Circ Physiol* **302**, H594–H602.

Oishi H, Budel S, Schuster A, Stergiopulos N, Meister JJ & Beny JL (2001). Cytosolic-free calcium in smooth-muscle and endothelial cells in an intact arterial wall from rat mesenteric artery in vitro. *Cell Calcium* **30**, 261–267.

Sandow SL (2004). Factors, fiction and endothelium-derived hyperpolarizing factor. *Clin Exp Pharmacol Physiol* **31**, 563–570.

Sandow SL, Goto K, Rummery NM & Hill CE (2004). Developmental changes in myoendothelial gap junction mediated vasodilator activity in the rat saphenous artery. *J Physiol* **556**, 875–886.

Sandow SL, Gzik DJ & Lee RM (2009*a*). Arterial internal elastic lamina holes: relationship to function? *J Anat* **214**, 258–266.

Sandow SL, Haddock RE, Hill CE, Chadha PS, Kerr PM, Welsh DG & Plane F (2009*b*). What's where and why at a vascular myoendothelial microdomain signalling complex. *Clin Exp Pharmacol Physiol* **36**, 67–76.

Sandow SL & Hill CE (2000). Incidence of myoendothelial gap junctions in the proximal and distal mesenteric arteries of the rat is suggestive of a role in endothelium-derived hyperpolarizing factor-mediated responses. *Circ Res* **86**, 341–346.

Sandow SL, Neylon CB, Chen MX & Garland CJ (2006). Spatial separation of endothelial small- and intermediate-conductance calcium-activated potassium channels (K(Ca)) and connexins: possible relationship to vasodilator function? *J Anat* **209**, 689–698.

Sandow SL, Tare M, Coleman HA, Hill CE & Parkington HC (2002). Involvement of myoendothelial gap junctions in the actions of endothelium-derived hyperpolarizing factor. *Circ Res* **90**, 1108–1113.

Schuster A, Beny JL & Meister JJ (2003). Modelling the electrophysiological endothelial cell response to bradykinin. *Eur Biophys J* **32**, 370–380.

Schuster A, Oishi H, Beny JL, Stergiopulos N & Meister JJ (2001). Simultaneous arterial calcium dynamics and diameter measurements: application to myoendothelial communication. *Am J Physiol Heart Circ Physiol* **280**, H1088–H1096.

Shimokawa H, Yasutake H, Fujii K, Owada MK, Nakaike R, Fukumoto Y, Takayanagi T, Nagao T, Egashira K, Fujishima M & Takeshita A (1996). The importance of the hyperpolarizing mechanism increases as the vessel size decreases in endothelium-dependent relaxations in rat mesenteric circulation. *J Cardiovasc Pharmacol* **28**, 703–711.

Siegl D, Koeppen M, Wolfle SE, Pohl U & de Wit C (2005). Myoendothelial coupling is not prominent in arterioles within the mouse cremaster microcirculation in vivo. *Circ Res* **97**, 781–788.

Silva HS, Kapela A & Tsoukias NM (2007). A mathematical model of plasma membrane electrophysiology and calcium dynamics in vascular endothelial cells. *Am J Physiol Cell Physiol* **293**, C277–C293.

Sokoya EM, Burns AR, Setiawan CT, Coleman HA, Parkington HC & Tare M (2006). Evidence for the involvement of myoendothelial gap junctions in EDHF-mediated relaxation in the rat middle cerebral artery. *Am J Physiol Heart Circ Physiol* **291**, H385–H393.

Taylor CW, Taufiq Ur R & Pantazaka E (2009). Targeting and clustering of IP_3 receptors: key determinants of spatially organized Ca^{2+} signals. *Chaos* **19**, 037102.

Tran CH, Taylor MS, Plane F, Nagaraja S, Tsoukias NM, Solodushko V, Vigmond EJ, Furstenhaupt T, Brighan M & Welsh DG (2012). Endothelial Ca2+ wavelets and the induction of myoendothelial feedback. *Am J Physiol Cell Physiol* **302**, C1226-C1242.

Tuttle JL & Falcone JC (2001). Nitric oxide release during alpha1-adrenoceptor-mediated constriction of arterioles. *Am J Physiol Heart Circ Physiol* **281**, H873–H881.

Yamamoto Y, Klemm MF, Edwards FR & Suzuki H (2001). Intercellular electrical communication among smooth muscle and endothelial cells in guinea-pig mesenteric arterioles. *J Physiol* **535**, 181–195.

Yashiro Y & Duling BR (2000). Integrated Ca^{2+} signaling between smooth muscle and endothelium of resistance vessels. *Circ Res* **87**, 1048–1054.

Author contributions

S.N., A.K., C.H.T., D.G.W. and N.M.T are responsible for conception and design of the research. S.N., A.K. and N.M.T implemented the models, performed the simulations, and drafted the manuscript. C.H.T. and D.G.W. edited and revised the manuscript. S.N., A.K., C.H.T., D.G.W. and N.M.T approved the final version of the manuscript.

Acknowledgements

This work was supported by the National Institutes of Health grant SC1HL095101 (N.M.T.), and an operating grant from the Canadian Institute of Health Research (D.G.W.). S.N. was supported by a Dissertation Year Fellowship from the University Graduate School of Florida International University.